

Cosmic Ray Origins in Supernova Blast Waves

A. R. Bell*

Clarendon Laboratory, University of Oxford, Parks Road, Oxford OX1 3PU, UK

ABSTRACT

We extend the self-similar solution derived by Chevalier (1983a) for a Sedov blast wave accelerating cosmic rays (CR) to show that the Galactic CR population can be divided into: (A) CR with energies above $\sim 200\text{GeV}$ released upstream during CR acceleration by supernova remnants (SNR), (B) CR advected into the interior of the SNR during expansion and then released from the SNR at the end of its life to provide the Galactic CR component below $\sim 200\text{GeV}$. The intersection between the two populations may correspond to a measured change in the Galactic CR spectral index at this energy (Adriani et al 2011).

Key words: cosmic rays, acceleration of particles, shock waves, magnetic field, ISM: supernova remnants

1 INTRODUCTION

Supernova remnants (SNR) are the most probable source of Galactic cosmic rays (CR) at energies up to a few PeV. CR gain energy at the outer shocks of supernova blast waves by first order Fermi diffusive shock acceleration (Krymsky 1977, Axford Leer & Skadron 1977, Bell 1978, Blandford & Ostriker 1978), although second order Fermi processes may also contribute (Ostrowski 1999). CR may also be accelerated by shocks associated with star formation, the large scale Galactic wind, or activity at the centre of the Galaxy.

Diffusive shock acceleration (DSA) efficiently produces a T^{-2} CR energy spectrum where T is the CR energy in eV. The predicted maximum CR energy produced by SNR shocks is close to a PeV, although it appears that the historical supernova remnants (SNR) are unable to reach this energy since their shocks are already significantly decelerated (Zirakashvili & Ptuskin 2008, Bell et al 2013). In order to explain the Galactic CR population it is essential not only that CR protons should be accelerated to a few PeV but also that the CR should be able to escape the SNR without large energy loss. Bell et al (2013) showed that the highest energy CR escape upstream from the shock into the interstellar medium. However most of the shock-accelerated CR, by energy content as well as number, are carried downstream into the interior of the SNR. In this paper we examine the fate of these lower energy CR as they are advected into the SNR where they remain until the SNR slows and disperses into the interstellar medium (ISM). Once carried into the SNR interior CR lose energy adiabatically as the SNR expands. An individual CR accelerated early in the Sedov phase has

a much reduced energy by the time it is released into the Galaxy. This is often perceived as a difficulty in explaining CR origins. However, the CR energy lost by adiabatic expansion is in fact re-used to drive the blast wave and accelerate a new generation of CR at a later time. Chevalier (1983a) derived a self-similar Sedov blast-wave solution that includes CR pressure. He showed that the CR pressure dominates the thermal plasma pressure at the centre of the remnant even if only a relatively small fraction of the available energy is given to CR by the shock. Because CR have a smaller ratio of specific heats ($\gamma = 4/3$) than thermal particles ($\gamma = 5/3$), CR lose less energy during adiabatic expansion. Thermal particles preferentially lose energy as they drive the blast wave and accelerate more CR, whereas CR preferentially keep their energy for release into the ISM at the end of the SNR's life.

In this paper we extend Chevalier's self-similar model to derive the CR energy spectrum and the maximum CR energy inside a blast wave. We show that CR produced by SNR can be divided into two populations: (A) CR with energies above $\sim 200\text{GeV}$ that escape ahead of the shock during SNR expansion (B) CR advected into the interior of the SNR during expansion and then released from the SNR at the end of its life to provide the Galactic CR component below $\sim 200\text{GeV}$. Instead of limiting the efficiency of Galactic CR production, adiabatic losses during SNR expansion increase the efficiency by filtering energy from the thermal plasma into CR. The underlying principles of the calculation apply to any blast wave, possibly including any launched from the centre of the Galaxy or from star forming regions.

Using the formulation developed by Bell et al (2013) we derive energy spectra and energy densities of CR within the SNR and the total energy of CR released into the surround-

* E-mail: t.bell1@physics.ox.ac.uk

ing medium. Bell et al (2013) showed that the maximum CR energy is determined by the growth rate of the instability amplifying the magnetic field needed to confine CR in the shock environment during acceleration. The results derived using Bell et al (2013) differ from those derived on an assumption that the energy density of the amplified magnetic field is proportional to the kinetic energy density $\rho_0 u_s^2$ of plasma with density ρ_0 overtaken by a shock with velocity u_s (eg Berezhko & Völk 2004, 2007). CR produced by SNR can be divided into populations A and B as defined above. The overlap of the two populations at an energy of about 200 GeV may be related to the break in the CR energy spectrum measured by PAMELA (Adriani et al, 2011) and other experiments (Ahn 2010, Tomassetti 2012).

Throughout this paper we consider only proton acceleration. Wherever CR are mentioned we refer to protons unless otherwise stated.

2 SEDOV SELF-SIMILARITY

In this section we derive the Sedov self-similar solution including the CR pressure as well as the thermal pressure. Chevalier (1983a) has previously derived this self-similar solution but we present the derivation in a form that facilitates calculation of the self-similar CR energy distribution inside the blast wave. A detailed time-dependent numerical study of the effect of efficient CR acceleration on SNR dynamics in the Sedov phase can be found in Castro et al (2011).

The essential feature of the Sedov solution for an expanding blast wave is that the total energy is conserved. At any time during self-similar expansion into a uniform medium with density ρ_0 the energy in the blast wave is proportional to $\rho_0 r_s^3 u_s^2$ since the energy density at any point inside the blast wave is proportional to $\rho_0 u_s^2$ (assuming that the shock Mach number is high) and the volume is proportional to r_s^3 where r_s is the radius of outer shock. From energy conservation $r_s^3 u_s^2$ is constant, so $r_s \propto t^{2/5}$ and $u_s \propto t^{-3/5}$.

In reality, and as part of this model, some energy is lost from the blast wave due to CR escaping upstream as estimated below in equation 19. **If the energy loss is self-similar in the sense that the total blast wave energy E decreases in proportion to $t^{-\beta}$ then $r_s \propto t^{(2-\beta)/5}$, $u_s \propto t^{-(3+\beta)/5}$, and $\beta = -2(dE/dr_s)/(5(E/r_s) - (dE/dr_s))$. If the energy loss due to CR escaping upstream is $0.03\rho_0 u_s^3$ per unit shock area (Bell et al 2013) then $dE/dr_s \approx -0.13E/r_s$ for $E \approx 3\rho_0 u_s^2 r_s^3$, which gives $\beta \approx 0.05$, $r_s \propto t^{0.39}$ and $u_s \propto t^{-0.61}$ instead of $r_s \propto t^{0.4}$ and $u_s \propto t^{-0.6}$.** This will produce a very slight flattening in the CR spectrum since it reduces the energy given to low energy CR later in the life of the SNR. Because the effect is small we neglect the effect of energy loss to CR and proceed on the assumption that $r_s \propto t^{0.4}$ and $u_s \propto t^{-0.6}$.

Self-similarity is independent of the ratio of specific heats γ . It also holds for a mixture of CR and thermal gases with different γ provided the CR acceleration efficiency is constant in time. We consider the case in which the immediately post-shock CR pressure P_{CR} is a fraction ϵ of the total post-shock pressure P_s with the thermal pressure P_t

providing the balance of the post-shock pressure:

$$P_{CR}(r_s) = \epsilon P_s \quad P_t(r_s) = (1 - \epsilon) P_s \quad (1)$$

In reality, ϵ probably varies as the shock speed changes, but for simplicity, and because it is unclear whether ϵ increases or decreases, we assume that it remains constant throughout the Sedov phase. For convenience and usefulness in later sections of this paper we introduce $R(r)$ as the radius of the shock when the fluid element presently at position r was overtaken by the shock. Since the mass presently inside the radius r is equal to the mass inside the shock when the shock was at radius R ,

$$\int_0^r 4\pi\rho(r')r'^2 dr' = \frac{4\pi}{3}\rho_0 R^3 \quad (2)$$

where ρ is the present density profile. $R(r)$ is a function of the present radius r . Since $u_s \propto r_s^{-3/2}$ the post-shock pressure was $(R/r_s)^{-3} P_s$ when the fluid element now at radius r passed through the shock. Hence the CR pressure at radius r is reduced by adiabatic expansion to $\epsilon P_s (R/r_s)^{-3} (\rho/\rho_s)^{4/3}$ where ρ_s is the post-shock density. Similarly the thermal pressure is $(1 - \epsilon) P_s (R/r_s)^{-3} (\rho/\rho_s)^{5/3}$ so the total pressure at radius r is

$$P = P_s \frac{r_s^3}{R^3} \left[(1 - \epsilon) \left(\frac{\rho}{\rho_s} \right)^{5/3} + \epsilon \left(\frac{\rho}{\rho_s} \right)^{4/3} \right] \quad (3)$$

where all quantities are defined at the present time. This equation assumes that all CR remain relativistic even as they cool adiabatically. In practice mildly relativistic CR become non-relativistic as they cool adiabatically and their γ changes from 4/3 to 5/3. We neglect this effect under the assumption that most of the CR energy resides in CR that remain relativistic. For example, if a T^{-2} spectrum extends to 1 PeV, CR with a Lorentz factor less than two account for only 6% of the total CR energy and CR with a Lorentz factor less than ten account for 15% of the total. See Chevalier (1983a,b) for a discussion of this issue when the shock-accelerated spectrum is steeper than T^{-2} .

We also assume that CR diffusion can be neglected and that CR remain localised to the same fluid element after passing through the shock. This is a good assumption for most CR, since CR are spatially localised by their small Larmor radius: the Larmor radius of a CR with energy T_{GeV} in GeV in a $10\mu\text{G}$ magnetic field is only $10^{-7} T_{GeV} \text{ parsec}$. Furthermore it is part of the theory of diffusive shock acceleration that all except the very highest energy CR exit the acceleration process by being advected away downstream with the thermal plasma. Hence advection dominates diffusion over most of the CR energy range, and diffusion can be neglected for bulk properties of CR such as the integrated energy density of all CR from the lowest to the highest energy.

From self-similarity, $\rho = \rho(r/r_s)$, the fluid velocity inside the SNR takes the form $u = t^{-3/5} f(r/r_s)$, and pressure takes the form $P = t^{-6/5} g(r/r_s)$ where f and g represent the shape of the velocity and pressure profiles. The self-similar equation for mass conservation is then

$$\frac{u_s r}{r_s} \frac{\partial \rho}{\partial r} = \frac{1}{r^2} \frac{\partial (r^2 \rho u)}{\partial r} \quad (4)$$

where the left hand side of the equation is the self-similar

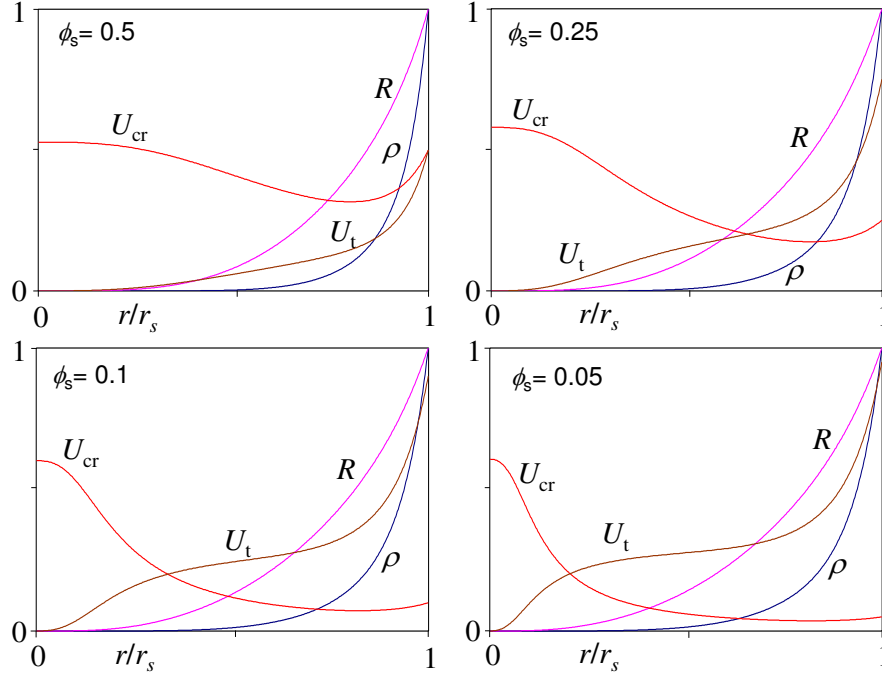


Figure 1. Profiles for different CR fractions ϕ_s . The axes are linear, not logarithmic.

equivalent of $-\partial\rho/\partial t$. The self-similar form of the momentum equation is

$$\frac{u_s r}{r_s} \frac{\partial u}{\partial r} + \frac{3u_s u}{2r_s} = u \frac{\partial u}{\partial r} + \frac{1}{\rho} \frac{\partial P}{\partial r} \quad (5)$$

where we have used equation 4 and the self-similar relation $u_s/r_s = 2/5t$. Equations 2-5 define the Sedov self-similarity solution with the CR pressure included where equations 2 and 3 combined represent energy conservation. The equation for mass conservation can be integrated to give

$$\frac{u}{u_s} = \frac{\rho r^3 - \rho_0 R^3}{\rho r^2 r_s} \quad (6)$$

The asymptotic solution close to the centre of the blast wave is derived in appendix A:

$$\frac{\rho}{\rho_s} = \left\{ \frac{1}{5(1-\epsilon)} \left[\left(16\epsilon^2 + \frac{10(1-\epsilon)\rho_s P_c r^3}{\rho_0 P_s r_s^3} \right)^{1/2} - 4\epsilon \right] \right\}^3 \quad (7)$$

where $P = P_c$ and $\partial P/\partial r = 0$ at zero radius. For $\epsilon \rightarrow 0$ (negligible CR pressure) $\rho \propto r^{9/2}$. For non-zero ϵ (CR dominant at the centre) $\rho \propto r^9$ as $r \rightarrow 0$. The asymptotic forms of R and u can be derived from equations 3, 6 and 7. Boundary conditions are imposed at the shock where

$$\rho_s = (4 + 3\epsilon)\rho_0 ; \quad P_s = \frac{3 + 3\epsilon}{4 + 3\epsilon}\rho_0 u_s^2 ; \quad R = r_s \quad (8)$$

We solve the equations numerically by integrating towards the centre from the shock radius r_s until numerical accuracy is lost close to $r = 0$ due to the density becoming very small ($\rho \propto r^9$ for small r). The profiles close to $r = 0$ are derived from the asymptotic solution given in equation 7 and fitted to the numerical solution by suitable choice of P_c . The resulting profiles are given in figure 1 for various shock acceleration efficiencies (see also Tables 1 to 5 of Chevalier (1983a)). We define ϕ as the ratio of the CR energy density

U_{CR} to sum of the thermal U_t and CR energy densities: $\phi = U_{CR}/(U_t + U_{CR})$. The subscript s denotes the value at the shock. ϵ and ϕ_s are related by

$$\phi_s = \frac{2\epsilon}{1 + \epsilon} ; \quad \epsilon = \frac{\phi_s}{2 - \phi_s} \quad (9)$$

and the post-shock thermal and CR energy densities are

$$U_{t,s} = \frac{18(1 - \phi_s)\rho_0 u_s^2}{(8 - \phi_s)(2 - \phi_s)} ; \quad U_{CR,s} = \frac{18\phi_s\rho_0 u_s^2}{(8 - \phi_s)(2 - \phi_s)} \quad (10)$$

In figure 1 we see that the thermal energy density always decreases towards the centre of the blast wave. In contrast, for all cases plotted in figure 1 the CR energy density is greater at the centre than immediately downstream of the shock. The central part of the blast wave can be characterised as a CR bubble with low thermal energy density and low mass density. The radius of the CR bubble decreases as the CR fraction ϕ_s decreases, but even when only 5 percent of the post-shock energy density is given to CR ($\phi_s = 0.05$) the CR bubble extends out to 10-20 percent of the shock radius. Adiabatic expansion inside the blast wave acts as a filter which transfers thermal energy to CR energy.

Figure 2 plots the CR, thermal and kinetic total energies as a function of ϕ_s (see also Table 6 of Chevalier (1983a)). It shows that as much as 70-80% of the total energy in the blast wave can be given to CR if CR acceleration at the shock is highly efficient. If equal energies are given to CR and thermal particles at the shock, CR contribute 53% of the total blast wave energy (thermal+CR+kinetic). Even if only 10% of the total CR plus thermal energy at the shock is given to CR, the CR energy in the blast wave is still 14% of the total. In the limit of small ϕ_s , the total energy of CR is $E_{CR} = 1.5\phi_s E_0 = 3\epsilon E_0$ where E_0 is the total energy of the blast wave. Far from reducing the efficiency of CR production, the hydrodynamics of the blast wave gives

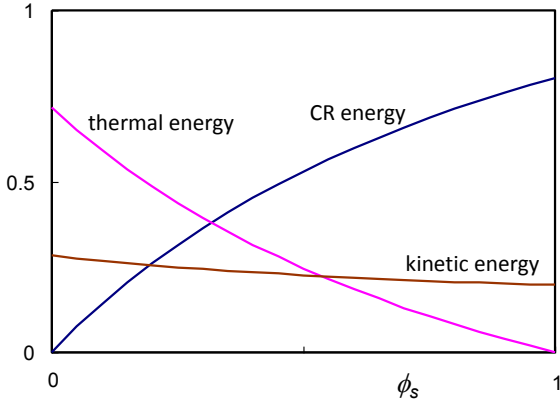


Figure 2. Fraction of total blast wave energy in CR, thermal and kinetic energy as a function of the fraction of energy $\phi_s = U_{CR,s}/(U_{t,s} + U_{CR,t})$ given to CR at the shock. See also Table 6 of Chevalier (1983a).

a proportion of the total blast wave energy to CR which is greater than the fraction ϕ_s of energy given to CR at the shock. Instead of being a problem for CR production, adiabatic expansion works to increase the fraction of the supernova energy given to CR. When a SNR finally disperses the CR energy released into the ISM may be a large fraction of the energy of the original explosion.

3 APPROACH TO SELF-SIMILARITY

$R(r)$ is the radius of the shock front at the time when the fluid element now at position r was overtaken by the shock. As seen in figure 1, a fluid element presently located about half way between the centre of the blast wave and the present shock radius was overtaken by the shock when it was only $\sim 10\%$ of its present radius. Consequently the early non-Sedov evolution of the blast wave affects a large part of its interior. Self-similarity cannot be naively assumed even when the blast wave has expanded to $10\times$ or even $100\times$ the radius r_f at which it completed the ejecta-dominated phase (sometimes known as the free expansion phase) and entered the Sedov phase. We characterise r_f as the radius at which the swept-up mass $4\pi\rho_0 r_f^3/3$ is equal to the ejected mass M_{ej} . Figure 3 provides insight into the late-time effect of the early pre-Sedov history of the blast wave. It plots $R(r)$ and the shock velocity $u_s(r)$ defined as the velocity of the shock at the time when the fluid element now at r was overtaken by the shock. Curves are plotted for different CR acceleration efficiencies: $\phi_s = 0.1$ and $\phi_s = 0.5$. u_s is plotted relative to its present value at $r = r_s$. For both values of ϕ_s the figure shows that a fluid element now at radius $r_s/2$ passed through the shock when the shock velocity was $\sim 30\times$ its present value. For example if the present shock velocity is 100km s^{-1} a fluid element at radius $r_s/2$ would have passed through the shock when its velocity was $\sim 3000\text{km s}^{-1}$. Fluid elements close to the centre of the blast wave would have been shocked at unrealistically high velocities. This casts doubt on the realism of the Sedov solution for the inner parts of the blast wave.

We examine the approach to Sedov self-similarity by

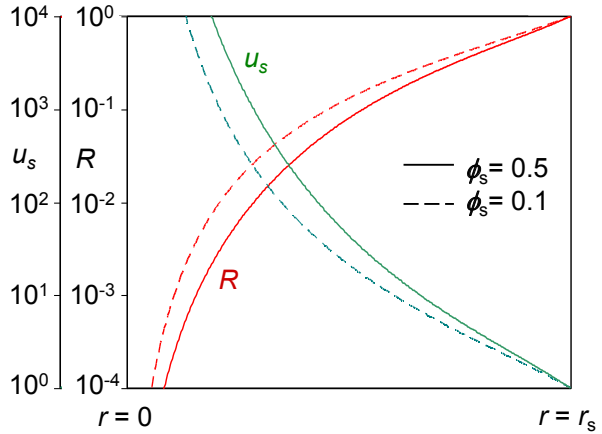


Figure 3. The curve for R plots the radius, relative to the present shock radius, at which fluid elements original passed through the shock. Similarly the curve for u_s plots the shock velocity, relative to the present shock velocity, when the fluid element now at radius r passed through the shock.

time-dependent Lagrangian hydrodynamic calculation of a blast wave driven by a thin spherical shell with mass M_{ej} initially expanding into a uniform medium of density ρ_0 with velocity u_{ej} . In reality the hydrodynamic structure of the early ejecta-dominated phase is much more complicated (Chevalier 1982, Truelove & McKee 1999). Ejecta are launched with a range of velocities rather than a single velocity u_{ej} but the thin shell model provides guidance on the validity of the Sedov model that is our concern here. The solution converges to the self-similar Sedov solution when the shock radius r_s is much greater than the radius r_f . The comparison is shown in figure 4 for $\phi_s = 0.25$ where the profiles of the mass density ρ , the CR energy density U_{cr} and the thermal energy density U_t are plotted when the blast wave has expanded to 10, 100 and 1000 times the radius r_f . The density profile is nearly unaffected by the pre-Sedov history. The energy densities are nearly unaffected when the blast wave has expanded by a factor of 1000 in radius, but strongly affected when the blast wave has expanded by a factor of 10. However, for all values of r_s/r_f in figure 4, the CR energy density exceeds the thermal energy density in the inner half (by radius) of the blast wave. Hence the conclusion of section 2 still stands that adiabatic expansion acts to filter energy into CR and the inner parts of the blast wave are dominated by CR pressure. The total pressure (CR plus thermal) at the centre of the blast wave is approximately independent of r_s/r_f in figure 4 since it is determined by the need to drive the blast wave into the surrounding medium.

In passing we note that the agreement between the curve for $r_s/r_f = \infty$ and $r_s/r_f = 1000$ in figure 4 for all except small radius where they would be expected to differ is evidence that both the self-similar and the thin shell calculations are reliable since the curves were calculated with different computer codes using different numerical methods.

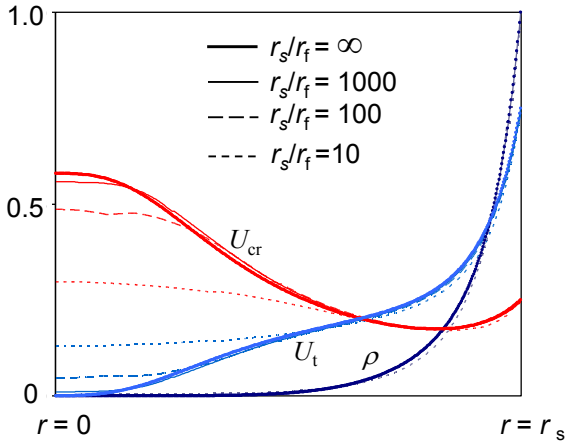


Figure 4. Profiles of the mass density, CR energy density and thermal energy density for $\phi_s = 0.25$. The self-similar solution is represented by the thick continuous lines. The other lines represent the approach towards self-similarity as the SNR radius r_s increases and an initial ejecta-dominated phase passes into history.

4 THE MAXIMUM CR ENERGY INSIDE THE BLAST WAVE

In this section we derive the maximum CR energy as a function of radius. We will assume self-similarity in this section and then examine effects arising from the pre-Sedov history in section 5. A fluid element presently at radius r passed through the shock when its radius was R . We assume that the CR accelerated by the shock followed a T^{-2} energy spectrum up to a maximum CR energy $T_s(R)$ in eV. After adiabatic expansion, the CR spectrum is still proportional to T^{-2} , but the maximum CR energy at radius r is reduced to

$$T_{max}(r) = T_s(R) \left(\frac{\rho}{\rho_s} \right)^{1/3} \quad (11)$$

$T_s(R)$ is determined by the microphysics of CR acceleration and the CR-driven amplification of magnetic field in the shock precursor. We consider three different models (A, B & C) for $T_s(R)$ as follows.

Equation 7 depends on the assumption that CR diffusion is small. While diffusion has negligible effect on bulk CR properties such as the CR energy density, as discussed in section 2, it could be more important for CR with energy T_{max} which have a relatively large Larmor radius. As discussed below the maximum CR energy in the centre of a SNR at the end of its life is about 10 TeV and these have a Larmor radius in a $10\mu\text{G}$ magnetic field of 0.001 parsec which is very much less than the SNR radius during the Sedov phase. Consequently, CR diffusion inside old SNR can only be important if the interior magnetic field is very small, and even then CR would be unable to escape through the larger compressed interstellar magnetic field closer to the shock. At early times during the Sedov phase T_{max} is larger but the magnetic field is also larger due to field amplification. Neglect of diffusion therefore seems reasonable, but the validity of the assumption might be tested with more complete calculations.

The dependence of $T_{max}(r)$ on $\rho(r)$ as given in equation 11 determines the maximum CR energy inside the blast wave

for a given maximum CR energy $T_s(R)$ at the shock. Bell et al (2013) showed that $T_s(R)$ in the early evolution of an SNR is determined by the growth rate of the instability that amplifies the magnetic field. Model C below is based on this understanding, but firstly for comparison we consider two other models, A and B, based on simpler ways of estimating $T_s(R)$ at the shock. Model A neglects magnetic field amplification during acceleration and assumes Bohm diffusion. Magnetic field amplification is well attested by observation as well as theory so Model B includes magnetic field amplification but still assumes Bohm diffusion. Model C both includes magnetic field amplification and avoids assuming Bohm diffusion.

Model A: Firstly we consider the option that $T_s = u_s B_0 r_s / 8$ which is derived from Lagage & Cesarsky (1983a,b) where B_0 is the upstream magnetic field (ie no magnetic field amplification ahead of the shock). This expression for T_s is based on Bohm diffusion (defined here as $D_{Bohm} = r_g c$ where r_g is the CR Larmor radius) in a magnetic field B_0 during shock acceleration. The factor 1/8 assumes that CR spend equal times upstream and downstream during acceleration (Bell 2013). Apart from the factor 1/8 this is also the maximum CR energy derived by Hillas (1984) for generalised CR acceleration. For self-similar expansion $u_s \propto r_s^{-3/2}$. Here and throughout the rest of the paper, for a SNR approaching the end of its life, we assume the following standard values:

$$B_0 = 5\mu\text{G} \quad u_s = 30\text{km s}^{-1} \quad r_s = 100\text{pc}.$$

The maximum CR energy at a radius r inside the blast wave is then

$$T_{max}(r) = 5 \left(\frac{R}{r_s} \right)^{-1/2} \left(\frac{\rho}{\rho_s} \right)^{1/3} \text{ TeV} \quad (12)$$

as plotted in figure 5, where R and ρ are functions of r . The curves labelled ‘model A’ in figure 5 show that the maximum CR energy falls away slowly inside the blast wave, but remains greater than 1 TeV until very close to the centre. With this recipe for the magnetic field, CR released into the ISM when a SNR reaches the end of its life can only replenish the Galactic CR population up to energies of a few TeV.

Model B: As pointed out by Lagage & Cesarsky (1983a,b) CR cannot be accelerated to PeV energies if the magnetic field at the shock is limited to interstellar values of a few μG . Magnetic field amplification (Bell 2004) facilitates CR acceleration to PeV energies. Option C will apply the latest theories of magnetic field amplification, but before that we consider the case in which $T_s = u_s B r_s / 8$ and the pre-shock magnetic field is amplified such that the magnetic energy density at the shock is a fixed fraction of the available energy, $B^2 / 2\mu_0 = \xi \rho_0 u_s^2$. Völk et al (2005) suggest from observations that the downstream magnetic energy density is $\sim 3\%$ of $\rho_0 u_s^2$ implying $\xi \sim 0.003$ (depending on the magnetic field orientation) when allowance is made for magnetic field compression at the shock (increasing B^2 by ~ 10) when estimating the upstream magnetic field. In this case, the upstream magnetic field is the maximum of the amplified field and a typical ISM field of $5\mu\text{G}$

$$\frac{B}{\mu\text{G}} = \max \left[5, 1.2 \left(\frac{\xi}{0.003} \right)^{1/2} \left(\frac{n_e}{\text{cm}^{-3}} \right)^{1/2} \left(\frac{u_s}{30\text{km s}^{-1}} \right) \right] \quad (13)$$

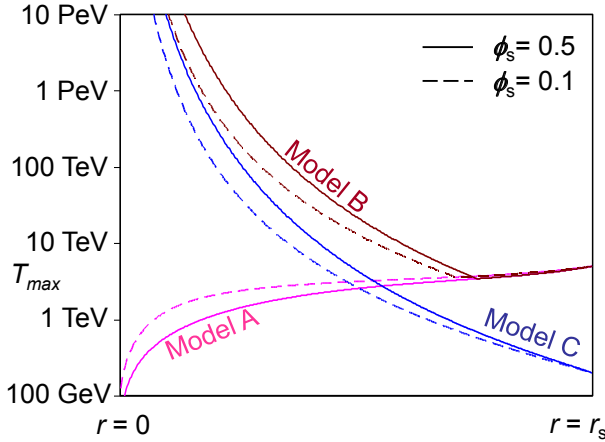


Figure 5. Maximum CR energy as a function of radius at the end of a SNR lifetime as given by Models A, B & C for $\phi_s = 0.5$ (full line) and $\phi_s = 0.1$ (dashed line).

The corresponding radial profile of the maximum CR energy for $B_0 = 5\mu G$, $u_s = 30\text{ km s}^{-1}$, and $r_s = 100\text{ pc}$ is

$$T_{max}(r) = \max \left[5.6 \left(\frac{R}{r_s} \right)^{-1/2}, 1.4 \left(\frac{R}{r_s} \right)^{-2} \right] \left(\frac{\rho}{\rho_s} \right)^{1/3} \text{ TeV} \quad (14)$$

as plotted in the curves labelled ‘model B’ in figure 5. T_{max} falls away for a small distance inside the shock before increasing dramatically at the centre of the SNR due to magnetic field amplification.

Model C: Model C is based on our current best understanding of magnetic field amplification as presented in Bell et al (2013). Models A and B based the calculation of T_{max} on the assumption of Bohm diffusion in a magnetic field that was unamplified in model A or deduced from observation in model B. Bell et al (2013) showed that the maximum CR energy in young SNR is more reliably determined by the growth rate of the instability responsible for magnetic field amplification. The non-resonant hybrid (NRH) instability dominates in young SNR. Its maximum growth rate is proportional to the electrical current carried by CR escaping upstream of the shock: $\gamma_{max} = 0.5j_{CR}\sqrt{\mu_0/\rho}$. For a given CR energy flux, the CR electric current is inversely proportional to the CR energy. This imposes a limit on energy to which CR can be accelerated since CR with very high energy carry a very small electric current for a given CR energy flux. A requirement of 5 e-foldings at the maximum growth rate means that the CR charge per unit area $j_{CR}\tau$ escaping a SNR with age τ must exceed $10\sqrt{\rho/\mu_0}$. By this argument, Bell et al (2013) derived an estimate (their equation 21) for T_{max} :

$$T_{max} = 230\eta_{0.03}n_e^{1/2}u_7^2R_{pc} \text{ TeV} \quad (15)$$

where u_7 is the shock velocity in units of $10,000 \text{ km s}^{-1}$, R_{pc} is the shock radius in parsec, n_e is the electron density in cm^{-3} and $\eta_{0.03}$ is an efficiency factor normalised relative to $\eta = 0.03$ as defined by Bell et al (2013) such that it is reasonable to assume that $\eta_{0.03} = 1$. This expression for T_{max} was based on the assumption that the magnetic field is strongly amplified by the NRH instability. This is correct for shock velocities greater than about $1,000 \text{ km s}^{-1}$ where the $j_{CR} \times B$

forces exerted by the CR current on the thermal plasma exceed the magnetic force $-B \times (\nabla \times B)/\mu_0$ acting within the thermal plasma. At shock velocities less than $\sim 1,000 \text{ km s}^{-1}$ the NRH instability is inactive (Schure & Bell 2013) and magnetic fluctuations are excited by the resonant Alfvén instability (Lerche 1967, Kulsrud & Pearce 1969, Wentzel 1974) that generates Alfvén waves with a wavelength $2\pi/k$ matching the CR Larmor radius r_g . The Alfvén instability operates differently from the NRH instability and dominates in a different regime but its maximum growth rate is a numerical factor times $0.5j_{CR}\sqrt{\mu_0/\rho}$. The numerical factor is close to one as noted by Zirakashvili & Ptuskin (2008) but depends upon the form of the CR energy distribution (see Appendix B). Hence the argument based on the NRH instability (Bell et al 2013) for high velocity shocks also applies to the Alfvén instability at low velocity shocks, and equation 15 can be applied to SNR throughout the Sedov phase. The corresponding profiles of T_{max} inside the blast wave are plotted as the curves labelled ‘model C’ in figure 5. T_{max} at a radius r is calculated from equation 15 with R_{pc} and u_7 set to the shock radius and shock velocity when the fluid element at r was overtaken by the shock.

The results obtained with models A, B & C are discussed further in the next two sections.

5 T_{MAX} NEAR THE CENTRE

According to figure 5 the maximum CR energy T_{max} is unbounded at zero radius in models B and C. This is an artifact due to the projection of self-similar Sedov expansion back to zero SNR radius. In the pre-Sedov ejecta-dominated phase, the shock velocity is much lower than that given by the Sedov model in which the expansion velocity is infinite at $t = 0$.

In section 3 (see figure 4) the effects of initial ejecta-dominated were estimated using a time dependent model in which the shock was driven by a thin shell representing the ejected mass M_{ej} . The same thin-shell model can be used to estimate T_{max} near the centre of the blast wave where the history of the ejecta-dominated phase is important. The shock velocity is nearly constant during the ejecta-dominated pre-Sedov phase and the radius is small initially so T_{max} turns over on approaching the centre of the blast wave as plotted in figure 6 in accord with equation 15. Nevertheless, T_{max} at the centre of the blast wave can be $\sim 100\text{--}1000$ times larger than T_{max} at the shock. In old SNR ($r_s/r_f = 100\text{--}1000$) CR energies may reach $\sim 10\text{--}100\text{ TeV}$ in the centre of an SNR even though CR are currently accelerated only to $\sim 100\text{ GeV}$ at the shock. Early in the Sedov phase ($r_s/r_f \sim 10$), T_{max} at the centre of the blast wave is only ~ 10 times larger than T_{max} at the shock.

6 THE LIMITATIONS OF MODELS A AND B

Models A and B predict larger CR energies than model C in the outer parts of the blast wave because they incorrectly assume Bohm diffusion in old SNR when the Alfvén instability is weakly driven. Bohm diffusion occurs when CR trajectories are scattered with a mean free path equal to the CR Larmor radius. This is only possible if rapidly growing

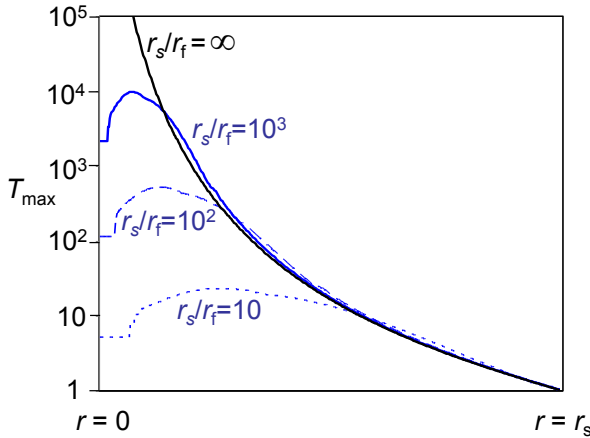


Figure 6. T_{max} at radius r within the SNR relative to T_{max} at the shock for model C with $\phi_s = 0.25$. r_s/r_f is the ratio of the SNR radius r_s to the radius r_f at the end of the ejecta-dominated phase. The Sedov self-similar result is given by $r_s/r_f = \infty$.

plasma instabilities produce large fluctuations in the field on the scale of a Larmor radius. If the magnetic field remains essentially uniform on the Larmor scale the CR are unscattered and diffusive shock acceleration is too slow for CR to reach the energy $u_s B_0 r_s / 8$ assumed in models A and B. Model C takes account of the instability growth time and consequently predicts the lower CR energies seen at large radius in figure 5. Models A and B therefore overestimate the CR energy at $r \sim r_s$ at the end of a SNR lifetime.

Model B also overestimates the maximum CR energy in the centre of the blast wave. Model B assumes that Bohm diffusion applies and that the Bohm diffusion coefficient should be calculated from the total magnetic field. In reality, fluctuations in the magnetic field grow on a wide range of scales from the Larmor radius of GeV protons to the Larmor radius of the highest energy CR. Bohm diffusion depends on a match between the Larmor radius of the scattered CR with the scalelength of the magnetic field. Only components of the magnetic field structured on the scale of the CR Larmor radius are effective in scattering a particular CR. The magnetic field derived from x-ray synchrotron emission at the shock (Berezhko et al 2003, Vink & Laming 2003, Völk et al 2005) is the total magnetic field. The component of the magnetic field on the Larmor radius of a particular CR is smaller. Model B uses the observed magnetic field as calculated by Völk et al (2005) to predict T_{max} and therefore model B overestimates the maximum CR energy. Compensation for this effect would probably reduce T_{max} in agreement with model C.

7 THE CR ENERGY SPECTRUM

The maximum CR energy T_{max} is plotted in figures 5 and 6 for different models as a function of radius r . Working on the basis that the energy spectrum at any radius follows a T^{-2} power up to the local maximum CR energy $T_{max}(r)$ we integrate in radius to calculate the differential energy spectrum of the total CR population inside the blast wave. The full lines in figure 7 present the CR spectrum calculated

for model C for two different CR acceleration efficiencies, ϕ_s equal to 0.1 and 0.5. The CR energy T is normalised to $T_{max,s}$ which is the current value of T_{max} at the shock. The spectrum is proportional to T^{-2} for $T < T_{max,s}$ since this power law applies at all points inside the blast wave in this energy range. The local maximum CR energy T_{max} increases towards the centre of the remnant so CR reach the highest energies only in a small volume close to the centre. Consequently the spectrum is steeper for $T > T_{max,s}$ but still follows a power law. The spectral index of 2.6 for $T > T_{max,s}$ is close to that of Galactic CR up to the knee, but this must be coincidental since the spectrum of CR arriving at the Earth is expected to be steepened by energy-dependent losses during propagation from the source. The shape of the spectrum is nearly independent of ϕ_s , but slightly flatter for $\phi_s = 0.1$.

The self-similar spectrum calculated for model C extends without limit towards infinite CR energy, representing CR acceleration by an infinitely fast Sedov blast wave expanding from a central singularity. The dashed curves in figure 7 plot the spectrum calculated with the time dependent code that models the pre-Sedov phase as described in sections 3 and 5. This more realistic thin-shell model of early expansion causes the CR spectrum to terminate instead of extend to infinite energy. The radius of a SNR expands by about 50 during the Sedov phase ($r_s/r_f \sim 50$) in which case the spectrum terminates at $\sim 200 T_{max,s}$ at the end of the Sedov phase. In other words, towards the end of the Sedov phase, CR near the centre of the SNR reach energies which are about 200 times larger than the maximum CR energy at the shock.

The total CR spectrum inside the SNR has two important energies: (i) the energy $T_{s,max}$ which is the maximum CR energy at the shock and at which the spectral index steepens from 2.0 to 2.6, (ii) $T_{t,max}$ which is the maximum CR energy anywhere in the SNR and the energy at which the spectrum terminates.

From equation 15, $T_{max,s} = 230 n_e^{1/2} u_7^2 R_{pc} \text{ TeV}$ where R_{pc} and u_7 are the shock radius and the shock velocity. The total energy of a Sedov blast wave is $E = 3 \rho_0 u_s^2 R^3$ for $\gamma = 5/3$ (the case of negligible CR pressure), so this formula can be re-cast as $T_{max,s} = 400 n_e^{1/6} E_{44}^{1/3} u_7^{4/3} \text{ TeV}$ where E_{44} is the blast wave energy in units of 10^{44} J . CR are only confined at the shock if the shock velocity is greater than the Alfvén speed v_A since the resonant Alfvén instability is only excited by CR drifting faster than the Alfvén speed. $v_A = 10 B_5 n_e^{-1/2} \text{ km s}^{-1}$ where B_5 is the magnetic field in units of $5 \mu\text{G}$. We make the assumption that CR are released into the ISM when the Alfvén Mach number decreases to 3 ($u_s = 3 v_A$) in which case $u_7 = 0.003 B_5 n_e^{-1/2}$ and

$$T_{max,s} = 200 n_e^{-1/2} E_{44}^{1/3} B_5^{4/3} \text{ GeV} \quad (16)$$

Under these assumptions, and with our standard parameters, CR are released into the ISM from the interior of the SNR at the end of its life with a power law spectrum T^{-2} at energies less than 200 GeV. At energies above 200 GeV the spectrum is steeper inside the blast wave and proportional to $T^{-2.6}$. The estimate of 200 GeV as the maximum energy to which CR are accelerated at the end of the SNR lifetime will be reduced if collisional damping in a dense partially ionised plasma inhibits the growth of CR-driven Alfvén waves as may be the case for the middle-aged SNR

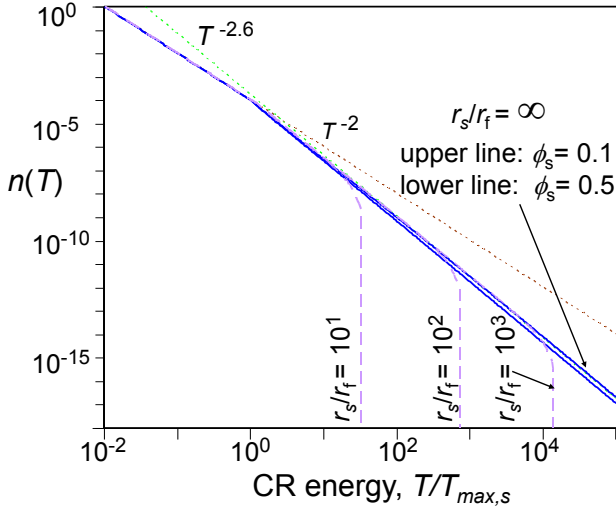


Figure 7. Energy spectra $n(T)$ integrated over all CR inside the blast wave as given by model C. The full lines refer to the self-similar model with $r_s/r_f = \infty$ and with $\phi_s = 0.5$ and $\phi_s = 0.1$. The dashed lines refer to the thin shell model with $\phi_s = 0.25$ and with the shock radius r_s equal to 10, 100 and 1000 times the ejecta-dominated radius r_f . The CR energy T is normalised to the current $T_{max,s}$ at the shock. The dotted lines are inserted as reference lines for T^{-2} and $T^{-2.6}$ power laws.

W44 where the proton spectrum turns over at only 10 GeV (Abdo et al 2010).

The energy $T_{max,t}$ at which the CR spectrum terminates can be estimated as follows. CR with the highest energy $T_{max,t}$ are found near the centre of the SNR (see figure 6). In the thin shell model they were accelerated as the SNR entered the Sedov phase. At that stage the shock velocity u_f was around $10,000 \text{ km s}^{-1}$ ($u_{f7} = 1$), the maximum CR energy was $T_{max,f} = 400 n_e^{1/6} E_{44}^{1/3} u_{f7}^{4/3} \text{ TeV}$ and the post-shock CR pressure was $P_f \approx 0.75 \epsilon \rho_0 u_f^2$. These initially very high energy CR cooled to the energy $T_{max,t}$ as the SNR expanded. By the time the CR are released into the ISM their pressure has decreased to $P_c \approx 0.25 \rho_0 u_s^2$ which is the pressure at the centre of a Sedov blast wave expanding at velocity u_s . Since individual CR energies reduce adiabatically in proportion to the CR pressure to the power $1/4$, $T_{max,t} = T_{max,f} (P_c/P_f)^{1/4} = T_{max,f} (u_s/u_f)^{1/2} (3\epsilon)^{-1/4}$. For our standard values, $T_{max,f} \approx 400 \text{ TeV}$, $u_f \approx 10,000 \text{ km s}^{-1}$, $u_s \approx 30 \text{ km s}^{-1}$, and $(3\epsilon)^{-1/4} \approx 1$, giving $T_{max,t} \sim 20 \text{ TeV}$. The implication of this very approximate estimate is that the maximum energy of CR released into the ISM from the interior of an SNR is about 20 TeV. Their energy is much less than the $\sim 400 \text{ TeV}$ to which they were originally accelerated in our simple model, and their numbers are relatively small because of the steeper energy spectrum ($T^{-2.6}$) above 200 GeV.

8 GALACTIC CR

In this paper we have shown that adiabatic losses do not reduce the total CR energy released into the ISM. Any energy lost by CR due to adiabatic expansion is used to drive the blast wave and accelerate a new generation of CR. In fact, adiabatic processes increase the overall efficiency of CR pro-

duction. Losses due to adiabatic expansion are stronger for the thermal plasma ($\gamma = 5/3$) than for CR ($\gamma = 4/3$). As shown in figures 1 & 2, most of the energy in the blast wave can be given to CR. The blast wave acts as a filter to accumulate CR which are then released into the ISM as the SNR eventually dissipates.

Adiabatic expansion operates to increase the total SNR energy passed to CR but it works against the production of CR with high energies reaching the knee in the spectrum. As estimated in section 7, the maximum CR energy $T_{max,t}$ inside the SNR at the end of its life is of the order of 20 TeV. SNR in the late Sedov phase may efficiently produce the Galactic CR population up to the maximum energy $T_{max,s}$ of CR being accelerated by the shock at the end of the SNR's life. As shown in figure 7, the CR spectrum inside the SNR steepens at this point before terminating at $T_{max,t}$. It was shown by Bell et al (2013) and Schure & Bell (2013) that CR above 200 GeV can instead be produced efficiently by young SNR, but these are released into the Galaxy by escaping upstream without passing into the interior of the SNR. They are the highest energy CR being accelerated by the shock at any time by the expanding SNR. They have long scattering mean free paths and carry the electrical current needed to excite instabilities upstream of the shock.

CR accelerated by SNR can therefore be divided into two populations. A high energy population (population A), extending from $\sim 200 \text{ GeV}$ to $\sim 1 \text{ PeV}$, escapes upstream with a T^{-2} energy spectrum when averaged over the Sedov phase. A low energy population (population B), with a T^{-2} energy spectrum below $\sim 200 \text{ GeV}$ and $T^{-2.6}$ between $\sim 200 \text{ GeV}$ and $\sim 20 \text{ TeV}$, is released into the ISM by old SNR after residing inside the remnant between acceleration and release. Although both populations contribute Galactic CR between $\sim 200 \text{ GeV}$ and $\sim 20 \text{ TeV}$, population A increasingly dominates toward the higher end of this range because of its flatter spectrum.

The production of the two CR populations is strongly related and they both have the same spectral index under the assumption that shock acceleration produces a T^{-2} spectrum. However their history between acceleration and release into the ISM is different so they may not connect seamlessly at the cross-over energy at $\sim 200 \text{ GeV}$. We assess the connectivity of the two populations by comparing the energy released into the ISM in each population.

Initially we compare the energy of each population in the limit of low acceleration efficiency in which ϵ is small. From section 2 and figure 2 the energy in low energy CR, population B, is

$$E_B \approx 3\epsilon E_0 \quad (17)$$

for small ϵ where E_0 is the total blast wave energy.

The energy released into the ISM as population A can be estimated from equations 2-4 from Bell et al (2013) in which CR escape ahead of the shock at energy T_{max} with electric current j_{CR} and consequent energy flux $j_{CR} T_{max}$. From these equations, the rate of CR energy escape from unit surface area of the shock is $0.75 P_{CR} u_s / \log(e T_{max} / m_p c^2)$ where P_{CR} is the CR pressure at the shock, u_s is the shock velocity and $e T_{max} / m_p c^2$ is the Lorentz factor of escaping CR protons. The total energy E_A released into the ISM with population A can be estimated by integrating over CR released as the SNR expands from the

radius R_f at the beginning of the Sedov phase to a radius R_s when CR are released into the ISM, giving

$$E_A = \int_{R_f}^{R_s} 4\pi R^2 \frac{0.75 P_{CR} u_s}{\log(eT_{max}/m_p c^2)} dt$$

$$\approx \frac{3\pi}{4} \frac{\log(R_s/R_f)}{\log(eT_{max}/m_p c^2)} \epsilon E_0 \quad (18)$$

$eT_{max}/m_p c^2 = 10^6$ for acceleration to 1PeV at the beginning of the Sedov phase, and $R_s = 50R_f$ for deceleration from $10,000 \text{ km s}^{-1}$ to 30 km s^{-1} during the Sedov phase in which $R_s \propto u_s^{-2/3}$, giving

$$E_A \approx 0.7 \epsilon E_0 \quad (19)$$

where $E_0 = 3\rho_0 u_s^2 R_s^3$. These estimates (equations 17 & 19) gloss over a number of complicating factors, but they are sufficient to suggest that the energies E_A and E_B in each population are comparable except that the energy in the higher energy population A is probably ~ 0.25 times that in population B. Hence the connection at around 200GeV can be expected to be reasonably smooth. If we take our estimates of E_A and E_B at face value, the spectrum at source below 200GeV is proportional to T^{-2} . At energies a little above 200GeV the spectrum steepens to $T^{-2.6}$ as seen in figure 7 before flattening again to T^{-2} as population A begins to dominate. Of course, the spectrum of CR arriving at the Earth is steepened due to energy losses during propagation. Also, the spectrum at source may deviate from a T^{-2} spectrum as discussed for example by Bell et al (2011).

The formula $E_B = 3\epsilon E_0$ is correct for small ϵ and ϕ_s . If CR acceleration is more efficient and $\phi_s = 0.5$ then the formula overestimates E_B by a factor of 2 (see figure 2). E_B and E_A are then closer in value but still $E_B > E_A$ and the overall picture of the Galactic CR spectrum is more or less unchanged.

Adriani et al (2011) find evidence in PAMELA data for a flattening in the Galactic CR spectral index above 200GeV. The detailed spectral structure observed at 200GeV might be open to question in the light of AMS data (Ting et al 2013), but the change in index is supported by other data (Ahn et al 2010, Tomassetti 2012). Our model suggests that the structure at 200GeV might be due to the joining of population A and population B. If anything we predict a local steepening above 200GeV rather than a flattening of the spectrum, and our prediction of the join occurring at 200GeV is uncertain easily by a factor of 2. However, it appears very likely that Galactic CR at PeV and GeV energies must have been accelerated at very different stages of SNR evolution and escaped into the interstellar medium by different routes at different times. More detailed modelling and observation is needed to establish whether the measured structure in the Galactic CR spectrum can be explained by our model or whether the answer lies in energy-dependent CR propagation from the SNR to the Earth as proposed for example by Blasi et al (2012) or Tomassetti (2012) or in spectral concavity due to non-linear effects as proposed by Ptuskin et al (2013).

9 OBSERVATIONAL CONSEQUENCES

Finally we briefly note some observational consequences for SNR and other blast waves. Our analysis predicts the existence of CR bubbles at the centres of older SNR as shown by Chevalier (1983a). These bubbles may extend 10s of parsec and extend half-way to the outer edge of the SNR. Inside the bubble, the CR energy density exceeds the thermal energy density, and the maximum CR energy T_{max} exceeds that of CR close to the shock. Despite the large CR energy density in the interior, CR protons are not strong emitters of γ -rays because of the low interior mass density and the consequent lack of thermal protons as targets for proton-proton interactions (see figure 1). CR electrons may be more detectable in the interior especially if they interact with a uniform photon density to emit inverse Compton radiation. The radio synchrotron luminosity in the interior is uncertain since it depends on the unknown magnitude of the magnetic field. The interior magnetic field is strongly reduced by adiabatic expansion but magnetic field amplification at the shock prior to expansion may compensate for this. Given the low predicted γ -ray emission by protons and the uncertainties in the radio emission, inverse Compton emission from CR electrons appears to be the most accessible signature of the presence of a CR bubble inside a blast wave.

The discussion presented in this paper may be applied to blast waves launched by any rapid energy release such as may occur in the centre of the Galaxy or any other galaxy, leading possibly to the formation of the Galactic Fermi bubbles (Carretti et al 2013) or the SNR-like shocks observed in Centaurus A (Croston et al 2009).

10 CONCLUSIONS

Our principal conclusions are that:

- SNR in the Sedov phase contain a CR bubble at their centre that extends to a quarter or a half of the SNR radius as previously shown by Chevalier (1983a).
- Adiabatic expansion serves to increase rather than decrease the efficiency of Sedov-phase SNR as producers of Galactic CR.
- Galactic CR can be divided into two populations: (A) CR at higher energies that escape upstream of the shock into the ISM as part of the acceleration process as discussed by Bell et al (2013), (B) CR with energies up to about 200GeV constituting CR bubbles that are released into the Galaxy at the end of the SNR's life.
- The intersection of the two populations may tentatively be identified with the change in spectral index detected by Adriani et al (2011) at $\sim 200\text{GeV}$.
- The CR electrons in the bubble may be detected by inverse Compton γ -rays but CR protons may be relatively undetectable due to the low mass density in the centre of blast wave. Synchrotron radio emission depends upon the magnetic energy density at the centre of a blast wave.
- The above discussion may be applicable to blast waves originating from the centres of our Galaxy or other galaxies.

11 ACKNOWLEDGEMENTS

I especially thank Brian Reville, Klara Schure and Gwenael Giacinti for many enlightening discussions relevant to this work; also Bojan Arbutina for interesting discussions during the National Conference of Astronomers of Serbia (Sept 2014), and an anonymous referee for helpful comments.

I thank the Aspen Center for Physics and the NSF Grant no.1066293 for hospitality during the workshop on "Astrophysical mechanisms of particle acceleration and escape from the accelerators", Sept. 1-15, 2013, organised by Mikhail Malkov.

The research leading to these results has received funding from the European Research Council under the European Community's Seventh Framework Programme (FP7/2007- 2013) / ERC grant agreement no. 247039 and from grants ST/H001948/1 and ST/K00106X/1 made by the UK Science Technology and Facilities Council.

12 REFERENCES

- Abdo A.A. et al, 2010, *Science* 327, 1103
 Achterberg A., 1983, *A&A*, 119, 274
 Adriani O., et al, 2011, *Science*, 332, 69
 Ahn HS et al, 2010, *ApJLett* 714, L89
 Axford W.I., Leer E. & Skadron G., 1977, *Proc 15th Int. Cosmic Ray Conf.*, 11, 132
 Bell A.R., 1978, *MNRAS*, 182, 147
 Bell A.R., 2004, *MNRAS*, 353, 550
 Bell A.R., 2013, *Astropart Phys* 43, 56
 Bell A.R., Schure K.M. & Reville B., 2011, *MNRAS*, 418, 1208
 Bell A.R., Schure K.M., Reville B. & Giacinti G., 2013, *MNRAS*, 431, 415
 Berezhko E.G., Ksenofontov L.T. & Völk H.J., 2003, *A&A* 412, L11
 Berezhko E.G. & Völk H.J., 2004, *A&A* 427, 525
 Berezhko E.G. & Völk H.J., 2007, *ApJLett* 661, L75
 Blandford R.D. & Ostriker J.P., 1978, *ApJ*, 221, L29
 Blasi P., Amato E. & Serpico P.D., 2012, *Phys Rev Lett* 109, 061101
 Carretti E. et al., 2013, *Nature* 493, 66
 Castro D., Slane P., Patnaude D.J. & Ellison D.C., 2011, *ApJ* 734, 85
 Chevalier, R.A., 1982, *ApJ* 258, 790
 Chevalier R.A., 1983a, *ApJ*, 272, 765
 Chevalier, R.A., 1983b, *Proc. 18th Int Cosmic Ray Conf (Bangalore)*, 2, 314
 Croston J.H. et al, 2009, *MNRAS*, 395, 1999
 Hillas A.M., 1984, *ARA&A* 22, 425
 Krymsky G.F., 1977, *Sov Phys Dokl*, 23, 327
 Kulsrud R. & Pearce W.P., 1969, *ApJ* 156 445
 Lagage O. & Cesarsky C.J., 1983a, *A&A* 118 223
 Lagage O. & Cesarsky C.J., 1983b, *ApJ* 125 249
 Lerche I., 1967, *ApJ* 147, 689
 Ostrowski M., 1999, *A&A* 345, 256
 Ptuskin V., Zirakashvili V. & Seo E-S., 2013, *ApJ* 763, 47
 Schure K.M. & Bell A.R., 2013, *MNRAS* 435, 1174
 Ting S., 2013, 'The AMS spectrometer on the *International Space Station*', Highlight Talk, 33rd Int Cosmic Ray Conf (Rio de Janeiro)

- Tomassetti N., 2012, *ApJL* 752, L13
 Truelove J.K. & McKee C.F., 1999, *ApJSS* 120, 299
 Vink J. & Laming J.M., 2003, *ApJ*, 584, 758
 Völk H.J., Berezhko E.G. & Ksenofontov L.T., 2005, *A&A*, 433, 229
 Wentzel D.G., 1974, *ARA&A* 12, 71
 Zirakashvili V.N. & Ptuskin V.S., 2008, *ApJ* 678, 939

APPENDIX A: THE SOLUTION AT SMALL RADIUS

In this appendix we derive the asymptotic profiles close to zero radius. Multiplying equation 3 by R^3/r_s^3 and differentiation with respect to radius gives

$$R^3 \frac{\partial P}{\partial r} + \frac{3\rho r^2}{\rho_0} P = \left(\frac{5}{3}(1-\epsilon) \left(\frac{\rho}{\rho_s} \right)^{2/3} + \frac{4}{3}\epsilon \left(\frac{\rho}{\rho_s} \right)^{1/3} \right) \frac{1}{\rho_s} \frac{\partial \rho}{\partial r} \quad (A1)$$

After rearrangement,

$$\left(3P + \frac{3 \int_0^r \rho r^2 dr}{\rho r^3} r \frac{\partial P}{\partial r} \right) r^2 = \frac{\rho_0 P_s}{\rho_s^2} \left(\frac{5}{3}(1-\epsilon) \left(\frac{\rho}{\rho_s} \right)^{-1/3} + \frac{4}{3}\epsilon \left(\frac{\rho}{\rho_s} \right)^{-2/3} \right) \frac{\partial \rho}{\partial r} \quad (A2)$$

From equation 5 $\partial P/\partial r \rightarrow 0$ as $r \rightarrow 0$ since $u \rightarrow 0$ as $r \rightarrow 0$ and $\partial u/\partial r$ is finite. The pressure must be non-zero at $r = 0$ since the motions are sub-sonic at the centre of the blast wave ($u \rightarrow 0$). Hence the term including $\partial P/\partial r$ can be neglected in equation A2. We define P_c as the pressure at $r = 0$ and integrate equation A2 with respect to r to obtain

$$\frac{5}{2}(1-\epsilon) \left(\frac{\rho}{\rho_s} \right)^{2/3} + 4\epsilon \left(\frac{\rho}{\rho_s} \right)^{1/3} - \frac{\rho_s P_c}{\rho_0 P_s} \left(\frac{r}{r_s} \right)^3 = 0 \quad (A3)$$

This quadratic in $(\rho/\rho_s)^{1/3}$ can be solved to obtain an expression for ρ which is reproduced in equation 7.

$$\frac{\rho}{\rho_s} = \left\{ \frac{1}{5(1-\epsilon)} \left[\left(16\epsilon^2 + \frac{10(1-\epsilon)\rho_s P_c r^3}{\rho_0 P_s r_s^3} \right)^{1/2} - 4\epsilon \right] \right\}^3 \quad (A4)$$

At the centre ($r \rightarrow 0$) $\rho \propto r^9$ unless $\epsilon = 0$ in which case $\rho \propto r^{9/2}$. The strong dependence of ρ on r strengthens the assertion above from equation 5 that $\partial P/\partial r$ can be neglected in equation A2.

APPENDIX B: THE MAXIMUM CR ENERGY AT A SHOCK

Equation 15 for the maximum CR energy at a shock was derived by Bell et al (2013) on the basis that a sufficient electric current must escape upstream of the shock to amplify the magnetic field through the growth of the NRH instability by about 5 e-foldings at its maximum growth rate. This determines the energy of the escaping CR since for a given CR energy flux set to a fixed fraction of ρu_s^3 the electric current is too small if the energy of CR carrying the current is very large. Conversely, if the energy of escaping CR is too low the CR current is large and the instability grows so rapidly that the magnetic field is strongly amplified and

the CR are unable to escape upstream. For more details of the model see Bell et al (2013).

The argument of Bell et al (2013) and the derivation of equation 15 for the maximum CR energy were based on the assumption that the NRH instability is active and dominant. This is true for young SNR with high shock velocities, but the NRH instability is inactive for SNR in the late Sedov phase. When the CR current drops below a characteristic value $j_c = B/(\mu_0 r_g)$ the $\mathbf{j}_{CR} \times \mathbf{B}$ force is too weak to overcome the tension in the magnetic field and the NRH instability ceases to operate. For a magnetic field of $5\mu\text{G}$ and an electron density of 1cm^{-3} , j_{CR} drops below the crossover value j_c when the shock velocity falls below $1,000\text{km s}^{-1}$. At shock velocities below this the Alfven instability (Lerche 1967, Kulsrud & Pearce 1969, Wentzel 1974) driven by CR streaming dominates. The Alfven instability causes the growth of Alfven waves in spatial resonance with the CR Larmor radius. Because Alfven waves are natural modes of the system they are undamped by tension in the magnetic field and can grow even if the growth rate drops below the natural frequency of the wave. The NRH and Alfven instabilities drive modes with opposite circular polarisations. In this appendix we set out the derivation of the maximum growth rates of both the Alfven and NRH instabilities for monoenergetic streaming CR using the formalism of Bell (2004), showing that the maximum growth rates for each instability are given by very similar expressions, differing only by 10 percent. The similarity of the two growth rates was previously noted by Zirakashvili & Ptuskin (2008).

Because of the similar growth rates the estimate of the maximum CR energy based on instability growth rates derived by Bell et al (2013) for the NRH instability at high shock velocities also applies to the Alfven instability at low shock velocities. Crucially for this paper, equation 15 can be applied to SNR throughout the Sedov phase.

The dispersion relation for CR-driven instability can be found in equation 7 of Bell (2004) (see also Achterberg (1983)). It includes both the Alfven and NRH instabilities. The dispersion relation is

$$\omega^2 = k^2 v_A^2 + (1 - \sigma) \frac{k j_{CR} B_{||}}{\rho} \quad (B1)$$

where k , j_{CR} (named $j_{||}$ in Bell (2004)) and $B_{||}$ are the wavenumber, CR electric current and magnetic field respectively, each aligned parallel to the shock normal. v_A is the Alfven speed. A small term in $\omega/k u_s$ has been omitted from equation 7 of Bell (2004) as justified therein. The function σ describes the response of the streaming CR to perturbations in the magnetic field. For monoenergetic CR with a Larmor radius r_g propagating diffusively relative to the background plasma, and $\lambda = 1/k r_g$,

$$\sigma = \frac{3}{4} \lambda (1 - \lambda^2) \left[\ln \left(\frac{\lambda + 1}{\lambda - 1} \right) \right] + \frac{3}{2} \lambda^2 \quad (B2)$$

for long wavelengths, $k < r_g^{-1}$, $\lambda > 1$, and

$$\sigma = \frac{3}{4} \lambda (1 - \lambda^2) \left[\ln \left(\frac{1 + \lambda}{1 - \lambda} \right) + i\pi \right] + \frac{3}{2} \lambda^2 \quad (B3)$$

for short wavelengths, $k > r_g^{-1}$, $\lambda < 1$. The imaginary term ($i\pi$) at short wavelengths results from the spatial resonance with the CR Larmor radius. No such resonance occurs at

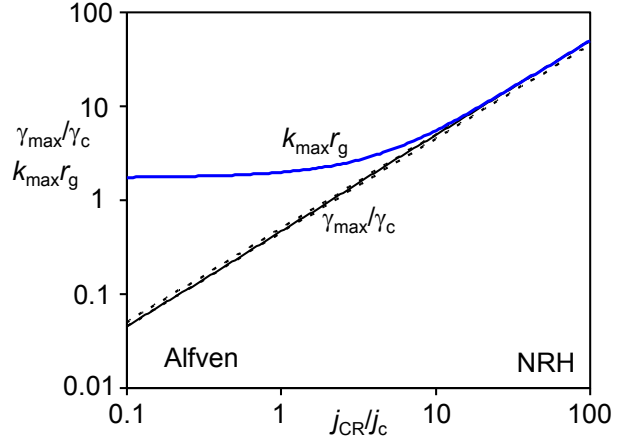


Figure 8. Plots of the maximum growth rate γ_{max} and the wavenumber k_{max} at which the growth rate is maximum against the CR current j_{CR} . k_{max} is normalised to the CR Larmor radius r_g . γ_{max} is normalised to $\gamma_c = v_A/r_g$. j_{CR} is normalised to $j_c = B/\mu_0 r_g$. The transition from the Alfven regime to the NRH regime occurs where $j_{CR} = 2\pi j_c$, ie when $j_{CR} = k_g B/\mu_0$ where $k_g = 2\pi/r_g$. The dotted lines correspond to the asymptotic limits $\gamma_{max} = 0.45\gamma_c(j_{CR}/j_c)$ and $\gamma_{max} = 0.5\gamma_c(j_{CR}/j_c)$ for the Alfven and NRH instabilities respectively.

wavelengths longer than the CR Larmor radius, which accounts for the absence of the imaginary term for $k r_g < 1$.

When the CR current j_{CR} is small and magnetic perturbations grow by the Alfven instability, $k^2 v_A^2$ dominates the real part of the right hand side of equation B1. In this limit, and with $k r_g > 1$,

$$\omega^2 = k^2 v_A^2 - \frac{3\pi i}{4} \left(\frac{k^2 r_g^2 - 1}{k^3 r_g^3} \right) \frac{k j_{CR} B_{||}}{\rho} \quad (B4)$$

In the limit of small j_{CR} , the maximum growth rate is

$$\gamma_{max} = \frac{\pi}{4} \sqrt{\frac{\mu_0}{3\rho}} j_{CR} = 0.45 \sqrt{\frac{\mu_0}{\rho}} j_{CR} \quad (B5)$$

which occurs when $k r_g = \sqrt{3}$.

In contrast, when the CR current j_{CR} is large and magnetic perturbations grow by the NRH instability, the maximum growth rate occurs at wavelengths much shorter than the CR Larmor radius ($\lambda \ll 1$). Both the real and imaginary parts of $\sigma \ll 1$ can then be neglected giving

$$\omega^2 = k^2 v_A^2 + \frac{k j_{CR} B_{||}}{\rho} \quad (B6)$$

In the appropriate polarisation, $k j_{CR} B_{||} < 0$,

$$\omega = \pm i \left(\frac{|k j_{CR} B_{||}|}{\rho} - k^2 v_A^2 \right)^{1/2} \quad (B7)$$

and the maximum growth rate is

$$\gamma_{max} = 0.5 \sqrt{\frac{\mu_0}{\rho}} j_{CR} \quad (B8)$$

which occurs when $|k| = 0.5 \mu_0 j_{CR} / B_{||}$.

Although the NRH and Alfven instabilities operate in different ways and in different polarisations, equations B5 and B8 show that the maximum growth is very similar in the low j_{CR} Alfven limit and the high j_{CR} NRH limit. The maximum growth rate for j_{CR} across the range from the

Alfven to the NRH limit is plotted in figure 8. To a good approximation the maximum growth rate can be assumed to be $0.5\sqrt{(\mu_0/\rho)}j_{CR}$ across the whole range of j_{CR} . Consequently, equation 15 provides a good estimate of the maximum CR energy at a shock at all times during the Sedov phase of SNR expansion.

The discussion in this appendix has treated the CR distribution as monoenergetic. This is reasonable for escaping CR which have to reach a certain energy before they escape and are not accelerated beyond this energy. Bell (2004) derives the dispersion relation for a T^{-2} CR distribution and similar results can be obtained from the plots of the real and imaginary parts of σ in figure 1 of that paper.